Supporting Information

Regulating Thermal Expansion of [FePt(CN)$_4$] Layer by Axial Coordination and Dimensional Reduction

Rui Ma,[δa] Liang Chen,[δa] Zhanning Liu,*[b] Kun Lin,[a] Qiang Li,[a] Weihua Ji,[c] Hankun Xu,[a] Xin Chen,[a] Jinxia Deng [a] and Xianran Xing *[a]

[a] Beijing Advanced Innovation Center for Materials Genome Engineering, Institute of Solid State Chemistry, University of Science and Technology Beijing, Beijing, 100083, China

[b] School of Materials Science and Engineering, Shandong University of Science and Technology, Qingdao, 266590, China

[c] College of Materials Science and Engineering, Taiyuan University of Technology, Taiyuan, 030024, China

E-mail: xing@ustb.edu.cn; znliu@sdust.edu.cn

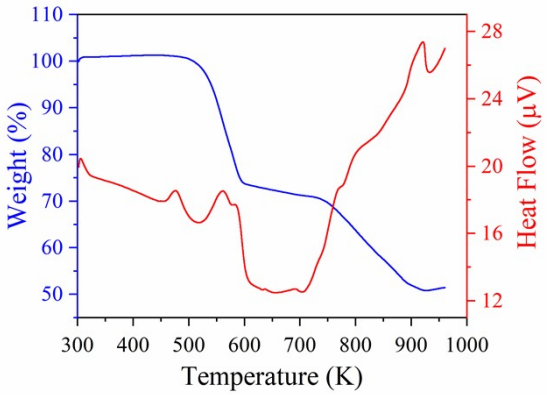

Figure S1. Thermogravimetric Differential Scanning Calorimetry (TG-DSC) curve for FePt_py.

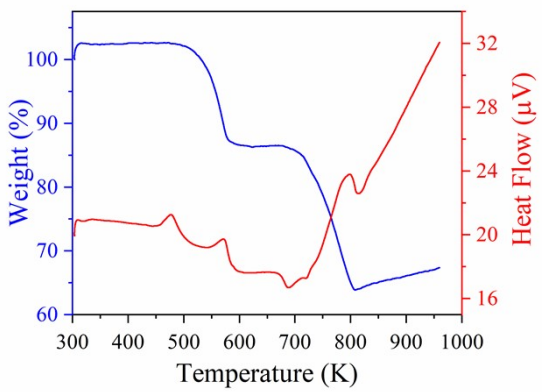

Figure S2. Thermogravimetric Differential Scanning Calorimetry (TG-DSC) curve for FePt_pyz.

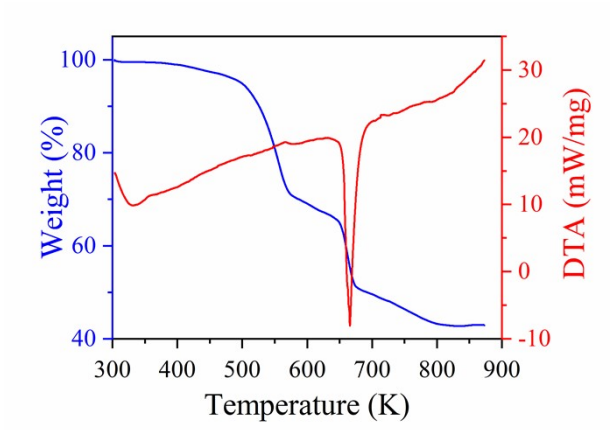

Figure S3. Thermogravimetric curve for FePt_pyz·I.

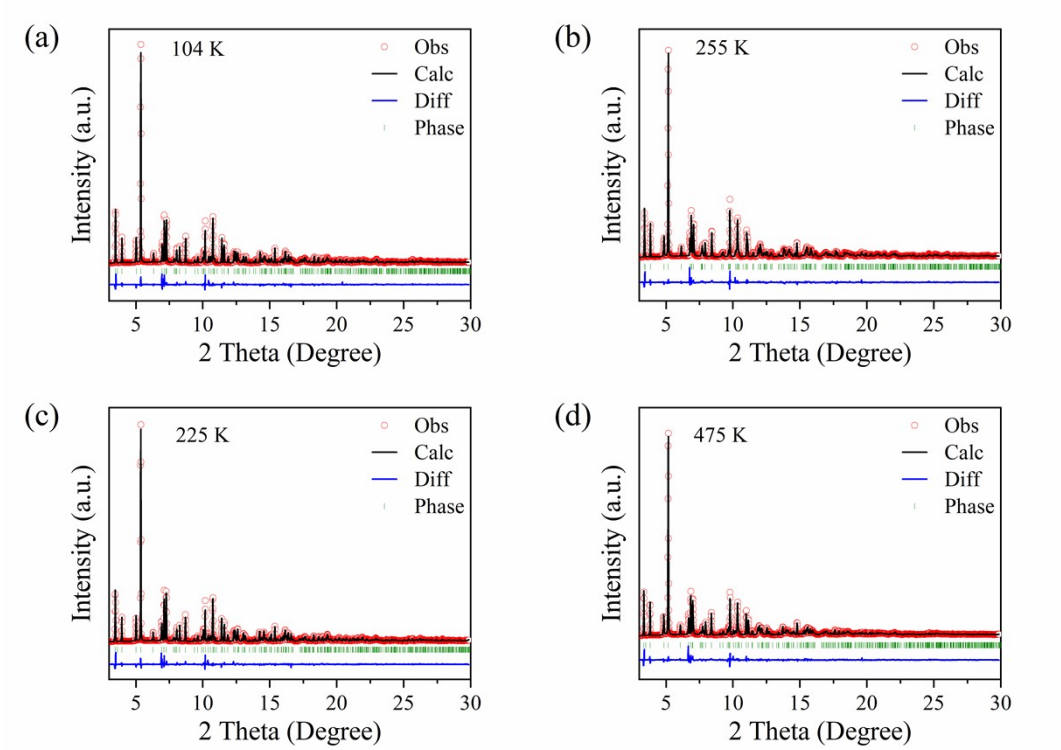

Figure S4. Rietveld Refinement to the synchrotron powder X-ray diffraction pattern of FePt_py at (a) 104 K and (c) 225 K in LS state and (b) 255 K and (d) 475 K in HS state.

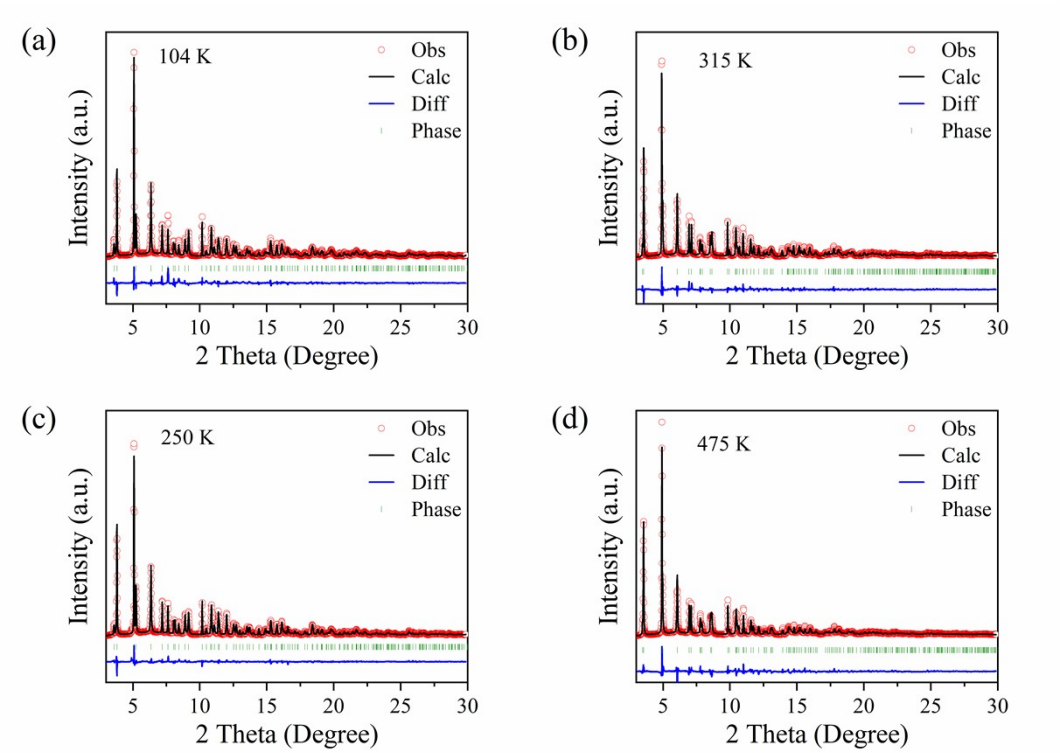

Figure S5. Rietveld Refinement to the synchrotron powder X-ray diffraction pattern of FePt_pyz at (a) 104 K and (c) 250 K in LS state and (b) 315 K and (d) 475 K in HS state.

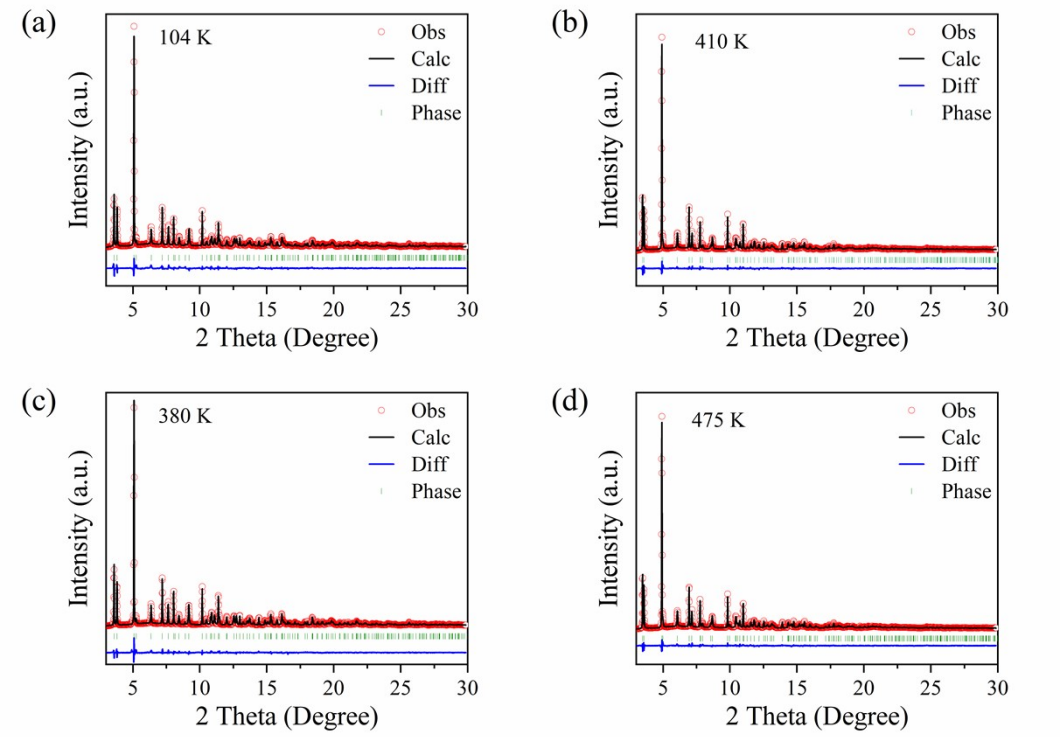

Figure S6. Rietveld Refinement to the synchrotron powder X-ray diffraction pattern of FePt_pyz·I, at (a) 104 K and (c) 380 K in LS state and (b) 410 K and (d) 475 K in HS state.

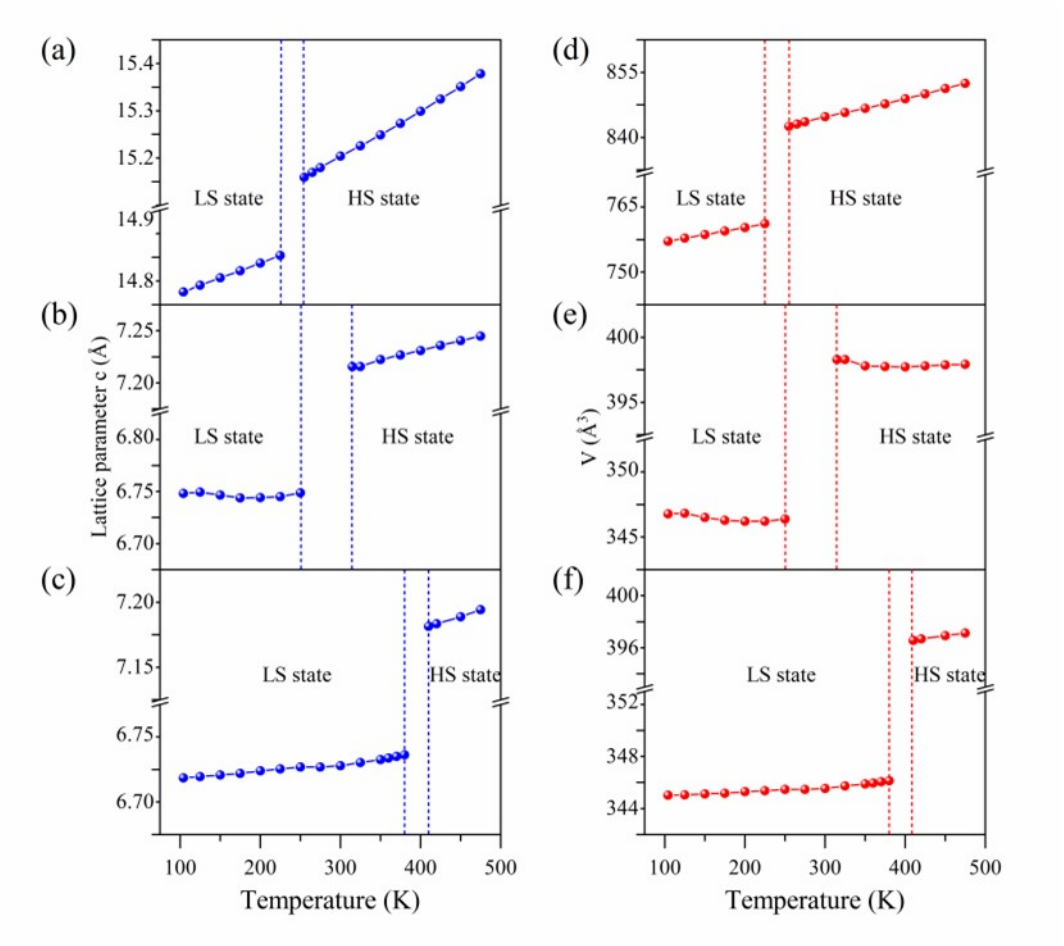

Figure S7. Temperature dependence of cell parameters *c* and V of FePt_py (a, d), FePt_pyz (b, e), and FePt_pyz•I (c, f)

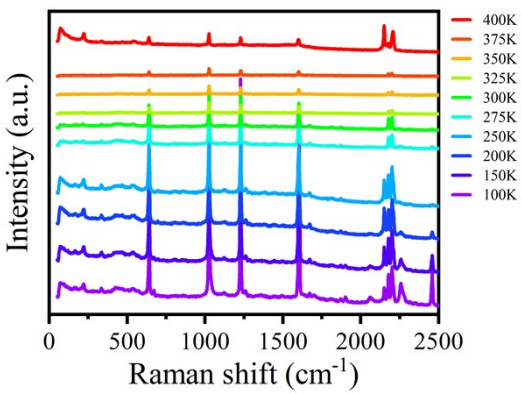

Figure S8. Variable temperature Raman spectra of FePt_pyz.

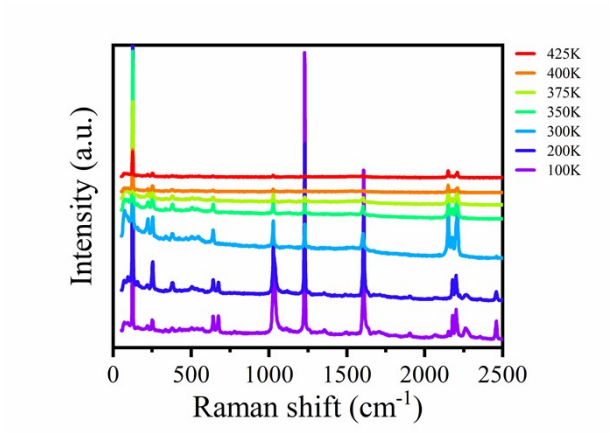

Figure S9. Variable temperature Raman spectra of FePt_pyz·I.